Monthly Notices of the ROYAL ASTRONOMICAL SOCIETY

MNRAS **525,** 4167–4175 (2023) https://doi.org/10.1093/mnras/stad2383
Advance Access publication 2023 August 07

Influences of dynamical disruptions on the evolution of pulsars in globular clusters

Kwangmin Oh,[1] C. Y. Hui,[2★] Jongsuk Hong,[3] J. Takata,[4] A. K. H. Kong,[5] Pak-Hin Thomas Tam,[6] Kwan-Lok Li[7] and K. S. Cheng[8]

[1]*Department of Space Science and Geology, Chungnam National University, Daejeon 34134, Republic of Korea*
[2]*Department of Astronomy and Space Science, Chungnam National University, Daejeon 34134, Republic of Korea*
[3]*Korea Astronomy and Space Science Institute, Daejeon 34055, Republic of Korea*
[4]*Department of Astronomy, School of Physics, Huazhong University of Science and Technology, Wuhan 430074, P. R. China*
[5]*Institute of Astronomy, National Tsing Hua University, Hsinchu 30013, Taiwan*
[6]*School of Physics and Astronomy, Sun Yat-sen University, Guangzhou 510275, P. R. China*
[7]*Department of Physics, National Cheng Kung University, Tainan 701401, Taiwan*
[8]*Department of Physics, The University of Hong Kong, Pokfulam Road 999077, Hong Kong*

Accepted 2023 July 31. Received 2023 July 24; in original form 2023 May 10

ABSTRACT

By comparing the physical properties of pulsars hosted by core-collapsed (CCed) and non-core-collapsed (non-CCed) globular clusters (GCs), we find that pulsars in CCed GCs rotate significantly slower than their counterparts in non-CCed GCs. Additionally, radio luminosities at 1.4 GHz in CCed GCs are higher. These findings are consistent with the scenario that dynamical interactions in GCs can interrupt angular momentum transfer processes and surface magnetic field decay during the recycling phase. Our results suggest that such effects in CCed GCs are stronger due to more frequent disruptions of compact binaries. This is further supported by the observation that both estimated disruption rates and the fraction of isolated pulsars are predominantly higher in CCed GCs.

Key words: binaries: general – pulsars: general – globular clusters: general.

1 INTRODUCTION

Millisecond pulsars (MSPs) are characterized by fast rotations with rotational periods $P_{\rm rot}$ typically shorter than a few tens of milliseconds and relatively weak surface magnetic fields $B_{\rm s} \lesssim 10^9$ G (Manchester et al. 2005; Hui & Li 2019). In order to achieve such fast rotation, MSPs are generally believed to have gone through an accretion phase, during which neutron stars gain angular momentum transferred from their companion stars (Alpar et al. 1982; Radhakrishnan & Srinivasan 1982; Fabian et al. 1983). This is commonly referred to as the recycling process. During recycling, mass accretion on the neutron star surface can potentially lead to magnetic field decay, as shown in Cumming, Arras & Zweibel (2004), which might account for the weak dipolar field strength inferred from observations.

MSPs can be further separated into two subgroups according to their locations: those residing in globular clusters (GCs) and those in the Galactic field (GF). Owing to the high stellar densities in GCs, the formation of MSPs inside a cluster can be influenced by intracluster dynamical processes (cf. Sigurdsson & Phinney 1995; Ivanova et al. 2008; Hui, Cheng & Taam 2010; Ye et al. 2019). While primary encounter interactions, such as tidal capture or direct collision with a giant, can facilitate binary formation (Fabian, Pringle & Rees 1975; Press & Teukolsky 1977; Lee & Ostriker 1986; Lombardi et al. 2006; Fregeau & Rasio 2007; Ye et al. 2022), subsequent encounters (referred to as secondary encounters hereafter) can play a role in disrupting binaries (Verbunt & Freire 2014).

Many studies have shown that dynamical interactions in GCs can lead to an increase in MSP population in comparison with the GF MSPs that rely on binary evolution alone (e.g. Ivanova et al. 2008; Hui et al. 2010; Ye et al. 2019). This is consistent with the well-known fact that the formation rate per unit mass of low-mass X-ray binaries (LMXBs), which are the progenitors of MSPs, is orders of magnitude larger in GCs than in GF (Clark 1975; Katz 1975). Although many more LMXBs can be assembled in GCs, the mass-transferring processes can be interrupted by the subsequent encounters. Such intricate dynamics could potentially lead to differences in the properties of MSPs in GCs compared to those in GF.

The sample sizes of the currently known populations of MSPs in GF and GCs are comparable, which allows a reasonable comparison of the properties between these two populations. In a recent study, Lee et al. (2023) performed a systematic comparison of rotational, orbital, and X-ray properties of MSPs in GCs and GF. They found that MSPs in GCs generally rotate slower than those in the GF. There is also an indication that the surface magnetic field of GC MSPs is stronger than those in the GF. These findings are consistent with the scenario that the recycling processes of GC MSPs were interrupted by secondary encounters, leading to shortened epochs for both angular momentum transfer and possible magnetic field decay.

★ E-mail: huichungyue@gmail.com, cyhui@cnu.ac.kr

Based on the photometric concentrations, GCs can be classified into core-collapsed (CCed) and non-core-collapsed (non-CCed; Harris 1996, 2010 edition). A core collapse in a GC is likely a result of gravothermal instability (cf. Lynden-Bell & Wood 1968), which can significantly affect the kinematic properties.

While the number of X-ray sources in GCs generally correlates with the primary encounter rate Γ (Pooley et al. 2003),[1] Bahramian et al. (2013) found that CCed GCs have fewer X-ray sources than non-CCed GCs for the same value of Γ (see fig. 9 in Bahramian et al. 2013). This might indicate the dynamical status of CCed GCs is different from that of non-CCed GCs, which can leave an imprint on the evolution of compact binaries. Therefore, it is reasonable to speculate that the properties of GC MSPs may be further diversified between CCed and non-CCed GCs.

Motivated by the aforementioned findings, we aim to explore potential differences in the properties of pulsars within CCed and non-CCed GCs by conducting a statistical analysis of selected parameters. In Section 2, we describe our procedure for preparing the data for analysis. The results of statistical analysis are given in Section 3 and their implications will be discussed in Section 4.

2 DATA PREPARATION

First, we have selected a sample of 280 pulsars from 38 different GCs from the Australia Telescope National Facility (ATNF) Pulsar Catalogue (Manchester et al. 2005, version 1.70). In this work, we only collected the following parameters from the catalogue: rotational period $P_{\rm rot}$, orbital period $P_{\rm b}$, and radio luminosity in L band $L_{1.4\,\rm GHz}$. On the other hand, we have adopted the X-ray luminosities $L_{\rm X}$ (0.3–8 keV) of 56 X-ray emitting MSPs from table 2 in Lee et al. (2023).

Observationally, it is a common practice to classify whether a GC is CCed or non-CCed based on its surface brightness profile (e.g. Trager, King & Djorgovski 1995; Harris 1996; Rivera Sandoval et al. 2018). Owing to the increased stellar density towards the cluster centre, a GC is defined as CCed if its surface brightness profile exhibits a power law until the limit of observational resolution (Trager et al. 1995; Rivera Sandoval et al. 2018). On the other hand, non-CCed GCs typically exhibit a flattened profile towards their centres and follow a King profile (King 1966; Trager et al. 1995).

In Section 3.1, we adopted the classifications given by Harris (1996, 2010 edition) in determining whether a GC is CCed or non-CCed. Using these labels, we divided our samples accordingly and compared their properties.

3 STATISTICAL ANALYSIS AND RESULTS

3.1 Core-collapsed GCs versus non-core-collapsed GCs

We conducted a detailed statistical analysis to compare the aforementioned selected properties of pulsars in CCed and non-CCed GCs. For each population, we first constructed the unbinned empirical cumulative distribution function (eCDF) of the parameters that are shown in Fig. 1. By visual inspection, these properties appear to be different between these two populations. To quantify the possible difference, we used a two-sample Anderson–Darling (A–D) test to investigate whether such differences are significant. In this work, we consider the difference between two eCDFs to be significant if the p-values inferred from the A–D test are <0.05. The results of the A–D test are summarized in Table 1.

We found that the distributions of $P_{\rm rot}$ and $L_{1.4\,\rm GHz}$ from CCed GCs and non-CCed GCs are significantly different. The corresponding p-values inferred from the A–D test are found to be 0.003 and 0.014, respectively. From the distributions of $P_{\rm rot}$ as shown in the upper right panel of Fig. 1, one can see that the pulsars in CCed GCs generally rotate slower than those in non-CCed GCs. The medians of $P_{\rm rot}$ in CCed and non-CCed populations are 5.24 and 4.45 ms, respectively.

For $L_{1.4\,\rm GHz}$, the distributions of these two groups of GC pulsars are obviously different (lower left panel of Fig. 1). It is very clear that the pulsars in the CCed GCs are more powerful radio emitters. The medians of $L_{1.4\,\rm GHz}$ in CCed and non-CCed are found to be 4.29 and 1.4 mJy kpc^2, respectively.

Fig. 1 suggests that $P_{\rm b}$ of the pulsars in CCed GCs are shorter, indicating that they have tighter orbits compared to those in non-CCed GCs. This finding is consistent with our understanding that pulsars with longer orbital periods in CCed GCs are more likely to have been disrupted by dynamical interactions. However, the p-value obtained from the A–D test is 0.24, which falls short of our pre-defined criterion for claiming a significant difference between the two groups. This result may be due to the small sample size.

While Lee et al. (2023) have compared the MSP properties between the GF and GC populations, and identified differences between them, they did not separately compare GF MSPs with those in CCed GCs and non-CCed GCs. To complement the analysis conducted by Lee et al. (2023) as well as our aforementioned investigations, we have further compared MSP properties among the populations in the GF, CCed GCs, and non-CCed GCs.

In comparing with the MSP properties in the GF, we have followed the same selection criterion as in Lee et al. (2023), by selecting pulsars with $P_{\rm rot} < 20$ ms in all three populations (i.e. GF, CCed GCs, and non-CCed GCs). This procedure can avoid including non-recycled GF pulsars in this part of the analysis. The eCDFs of $P_{\rm rot}$, $P_{\rm b}$, $L_{1.4\,\rm GHz}$, and $L_{\rm X}$ are shown in Fig. 2. The results of the A–D test are summarized in Table 1.

From the distribution of $P_{\rm rot}$, it is obvious that the rotation of MSPs in the GF is significantly faster than those in CCed and non-CCed GCs. Moreover, we can see that the difference between CCed GCs and GF is larger than that between non-CCed GCs and GF. We also find that the $P_{\rm b}$ of GF MSPs is significantly longer than those in GCs, regardless of whether they are CCed or non-CCed. All these findings align with the scenario suggested by Lee et al. (2023), which posits that intracluster dynamics have resulted in the formation of more tightly bound binaries and the interruptions of the recycling process.

For comparing the distributions of luminosities between GF and GC MSPs in X-ray and radio, we found differences that are statistically acceptable (see Table 1). However, given the current sample, it is difficult to rule out the possibility that such differences have resulted from the observational bias between GF and GCs (see the discussion in Section 4).

Since $P_{\rm rot}$ and $L_{1.4\,\rm GHz}$ of the MSPs in CCed GCs are found to be significantly different from those in non-CCed GCs and the GF, we have further examined their distributions by computing the kernel density estimates (KDEs). The results are shown in Fig. 3. In the panel of $P_{\rm rot}$, it clearly shows that the peaks of density distributions systematically shifted towards the larger value from the GF (which lacks dynamical interactions) to the CCed GCs (which have the largest disruption rates among three populations; see Table 2). The peaks for the KDEs of $P_{\rm rot}$ for GF, non-CCed GCs, and CCed GCs are 3.6, 4.6, and 5.0 ms, respectively. For $L_{1.4\,\rm GHz}$, the KDEs of GF and CCed GC populations peaked at 1.8 and 2.8 mJy kpc^2, respectively.

[1] $\Gamma \propto \rho_{\rm c}^{1.5} r_{\rm c}^2$, where $\rho_{\rm c}$ and $r_{\rm c}$ are the density and radius of the cluster core, respectively.

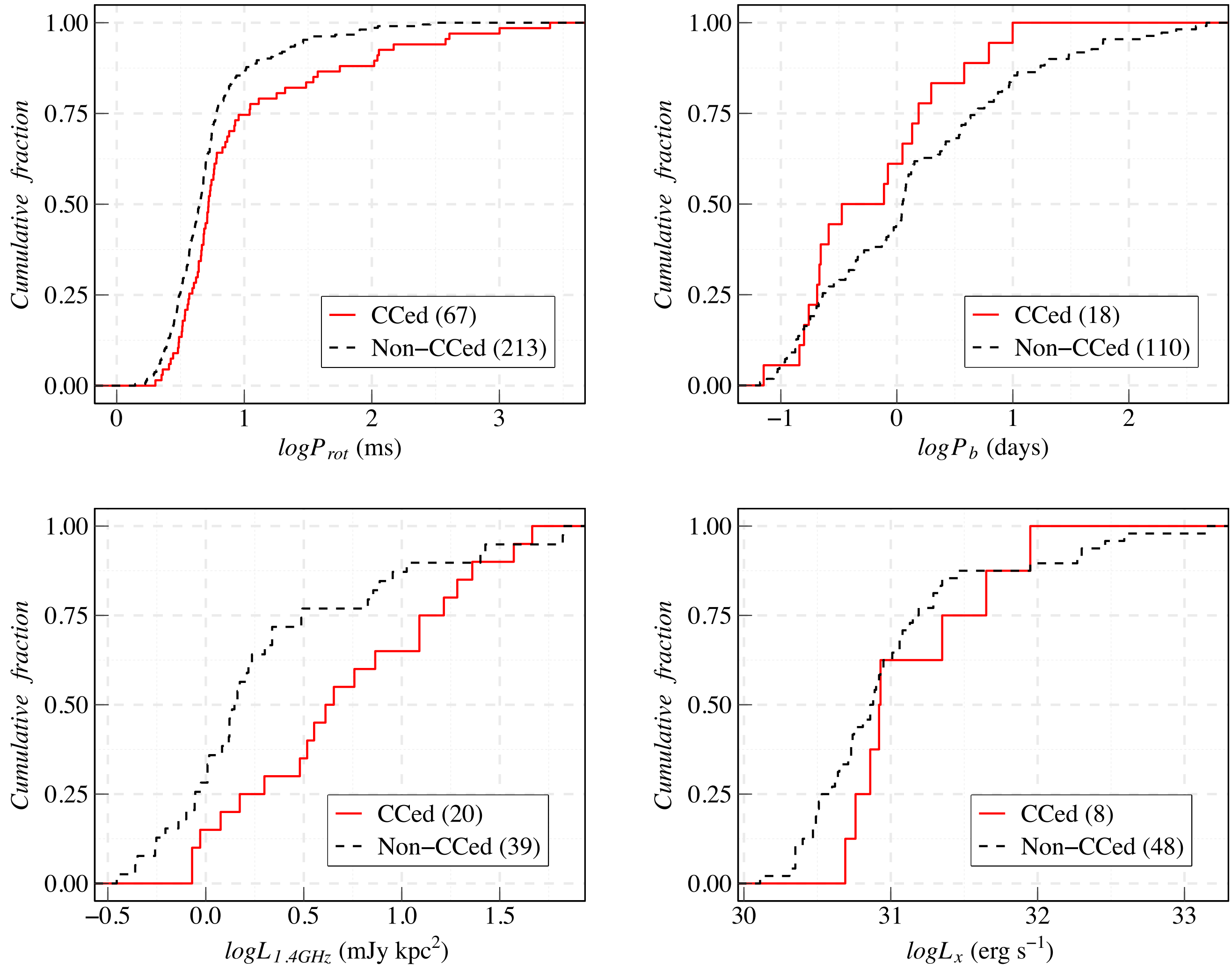

Figure 1. Comparisons of eCDFs of the selected pulsar properties between CCed GCs and non-CCed GCs. The numbers in parentheses in the legends show the corresponding sample sizes.

Table 1. Null hypothesis probabilities of the Anderson–Darling (A–D) test for comparing $P_{\rm rot}$, $P_{\rm b}$, $L_{1.4\,{\rm GHz}}$, and $L_{\rm X}$ among CCed GCs, non-CCed GCs, and GF.

	CCed versus non-CCed[a]	CCed versus GF[b]	Non-CCed versus GF[b]	GCs versus GF[c]
$P_{\rm rot}$	0.003	0.002	0.023	0.001
$P_{\rm b}$	0.242	0.001	9×10^{-5}	10^{-7}
$L_{1.4\,{\rm GHz}}$	0.014	0.001	0.094	0.041
$L_{\rm X}$	0.315	0.137	0.078	0.030

Notes. [a]Cf. Fig. 1.
[b]Cf. Fig. 2.
[c]GCs = CCed + non-CCed.

In the case of non-CCed GC MSPs, it is interesting to note that there appear to have two peaks in its $L_{1.4\,{\rm GHz}}$ KDE that is located at 1.3 and 8.0 mJy kpc^2. However, there are only seven non-CCed GC MSPs $\gtrsim 3$ mJy kpc^2 in the current sample that does not allow us to determine whether such multimodal distributions are genuine or simply a fluctuation due to the small sample.

Verbunt & Freire (2014) have compared the fraction of isolated pulsars in GCs with the corresponding disruption rate $\gamma \propto \rho_{\rm c}^{0.5} r_{\rm c}^{-1}$, where $\rho_{\rm c}$ and $r_{\rm c}$ represent the central density and core radius, respectively (cf. table1 in Verbunt & Freire 2014). In their work, they considered a sample of only 14 GCs. Since our sample is now almost three times larger, it is legitimate to revisit this comparison. For computing γ, we adopted ρ_0 and $r_{\rm c}$ from Harris (1996, 2010 edition). In Table 2, we compare the numbers of isolated pulsars $N_{\rm s}$ and binary pulsars $N_{\rm b}$ in 37 GCs with their corresponding γ. GLIMPSE01 is excluded in this part of the analysis because we cannot find its structural parameters in the literature.

We proceeded to examine if there is any correlation between the fraction of isolated pulsars $f_{\rm s} = N_{\rm s}/(N_{\rm s} + N_{\rm b})$ and γ with the non-parametric Spearman's rank test, which yields a p-value of 0.014. This indicates the correlation between these two quantities is significant. This prompts us to perform a regression analysis to obtain an empirical relation between $f_{\rm s}$ and γ. However, in view of the small statistics of pulsar population in most GCs, we notice that the $f_{\rm s}$ is very sensitive to $N_{\rm s}$ and $N_{\rm b}$. In particular, many of the GCs have $f_{\rm s} = 0$ (Table 2).

To address this issue, we found that Laplace smoothing is a well-established technique in handling categorical data with a small sample size (e.g. Manning, Raghavan & Schütze 2008; Gelman et al. 2013). By adding a smoothing parameter α to the observed counts, the method can stabilize the estimates and avoid zero empirical

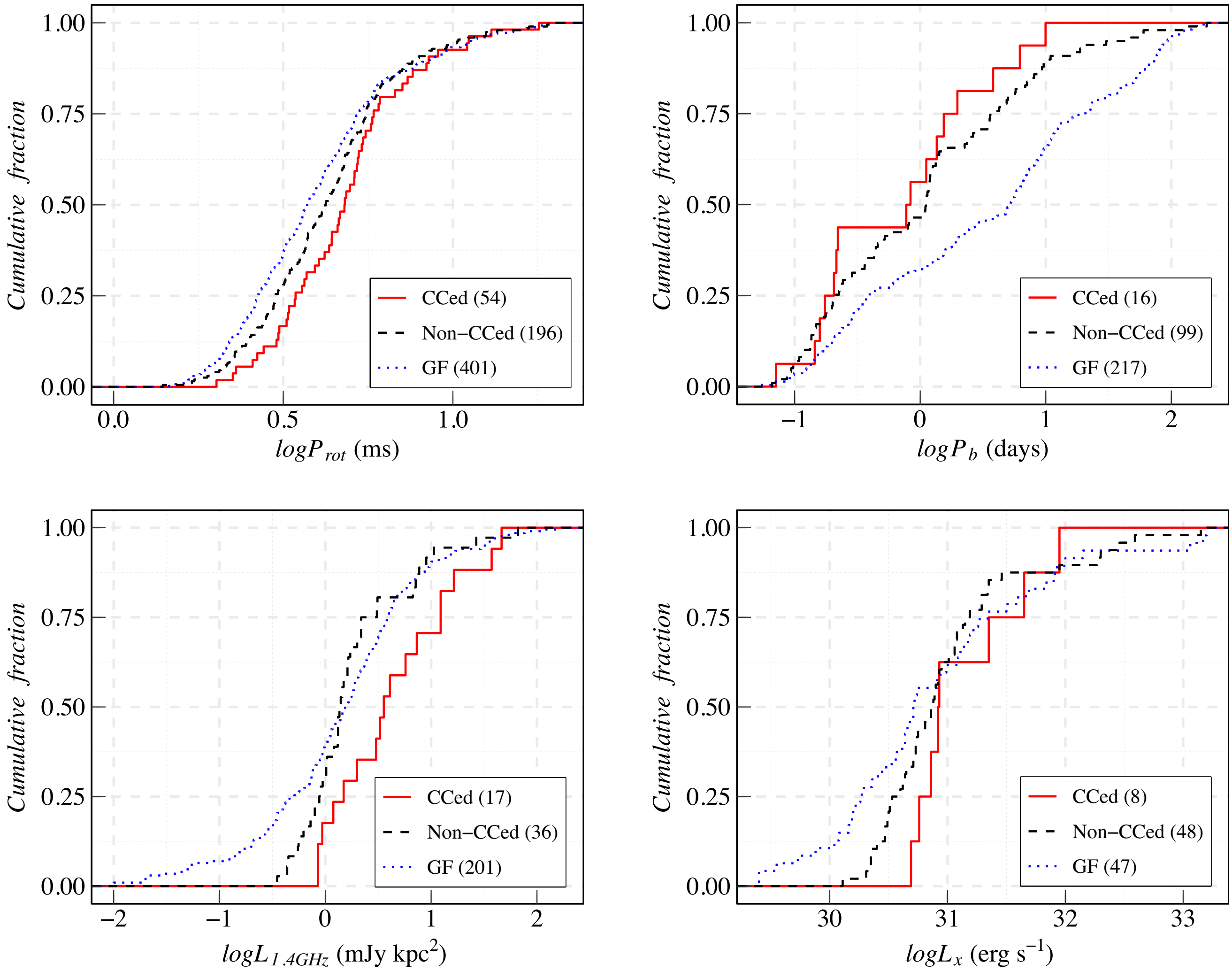

Figure 2. Comparisons of eCDFs of the selected pulsar properties among CCed GCs, non-CCed GCs, and GF. The numbers in parentheses in the legends show the corresponding sample sizes.

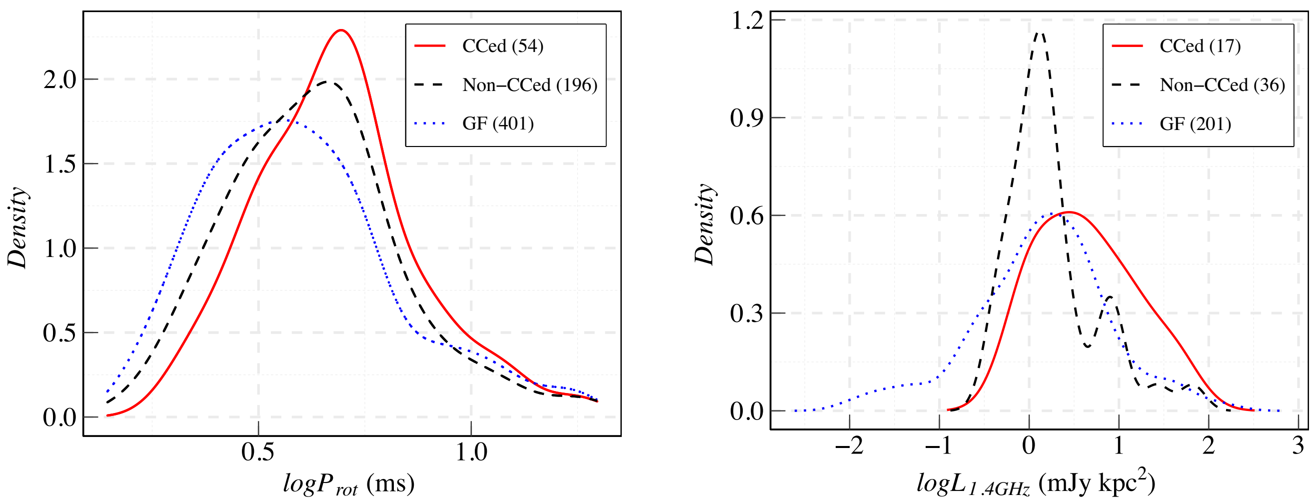

Figure 3. KDEs for the distributions of log $P_{\rm rot}$ and log $L_{1.4\,\rm GHz}$ of MSPs in CCed GCs, non-CCed GCs, and the GF.

Table 2. Updated statistics of single and binary pulsars as well as the structural parameters of GCs.

Name	N_b	N_s	r_c (pc)	$\log \rho_c$ ($L_\odot$ pc^{-3})	γ ($\gamma_{M\,4}$)	Class
			Non-CCed GCs			
47 Tuc	19	10	0.36	4.88	6.57	I
M 10	2	0	0.77	3.54	0.67	S
M 12	2	0	0.79	3.23	0.42	S
M 13	4	2	0.62	3.55	0.52	S
M 14	5	0	0.79	3.36	0.25	S
M 2	6	0	0.32	4.00	1.05	I
M 22	2	2	1.33	3.63	0.59	S
M 28	10	4	0.24	4.86	7.88	I
M 3	6	0	0.37	3.57	0.62	I
M 4	1	0	1.16	3.64	1.00	I
M 5	6	1	0.44	3.88	1.02	I
M 53	4	1	0.35	3.07	0.21	S
M 71	5	0	0.63	2.83	0.40	S
M 92	1	0	0.26	4.30	2.53	I
NGC 1851	9	6	0.09	5.09	12.44	I
NGC 5986	1	0	0.47	3.41	0.40	S
NGC 6440	4	4	0.14	5.24	13.53	I
NGC 6441	3	6	0.13	5.26	10.93	I
NGC 6517	3	14	0.06	5.29	26.82	I
NGC 6539	1	0	0.38	4.15	1.55	I
NGC 6652	2	0	0.1	4.48	6.71	I
NGC 6712	1	0	0.76	3.18	0.29	S
NGC 6749	2	0	0.62	3.30	0.35	S
NGC 6760	1	1	0.34	3.89	1.35	I
Omega Cen	8	10	2.37	3.15	0.12	S
Terzan 5	24	20	0.16	5.14	13.00	I
			CCed GCs			
M 15	1	8	0.14	5.05	8.89	D
M 30	2	0	0.06	5.01	25.42	D
M 62	9	0	0.22	5.16	9.82	I
NGC 362	5	1	0.18	4.74	5.85	I
NGC 6342	1	1	0.05	4.97	27.76	D
NGC 6397	2	0	0.05	5.76	254.79	D
NGC 6522	0	6	0.05	5.48	55.13	D
NGC 6544	3	0	0.05	6.06	275.92	I
NGC 6624	2	10	0.06	5.30	36.40	D
NGC 6752	1	8	0.17	5.04	18.81	D
Terzan 1	0	7	0.04	3.85	12.13	D

Note. Number of binary pulsars N_b and isolated pulsars N_s from Manchester et al. (2005). Core radius r_c and central luminosity density ρ_c from Harris (1996, 2010 edition). Disruption rates $\gamma \propto \rho_c^{0.5} r_c^{-1}$ from equation (2) in Verbunt & Freire (2014), which are normalized with the value of M 4. The class labels in the seventh column represent the groups of sparse (S), intermediate (I), and dense (D) as determined by Gaussian mixture model (GMM; see Section 3.2).

probabilities. With Laplace smoothing, we obtained the smoothed estimate of f_s as $\hat{f}_s = \frac{N_s+\alpha}{N_s+N_b+2\alpha}$ with α taken to be 1.

In Fig. 4, we show the scatter plot between $\hat{f}_s$ and $\log \gamma$ of our sample. It is obvious that the disruption rates of CCed GCs are generally larger than those of non-CCed GCs. Furthermore, GCs with $\hat{f}_s \gtrsim 0.5$ are predominantly CCed GCs with γ more than 10 times larger than the conventional reference level in M 4. These findings are fully consistent with the results reported by Verbunt & Freire (2014). By fitting a linear model $\hat{f}_s = a \log \gamma + b$ to the data with each GC weighted by the numbers of detected pulsars, we found the best-fitting parameters of $a = 0.12 \pm 0.05$ and $b = 0.38 \pm 0.05$ (1σ uncertainties) for this empirical relation. To test whether the result

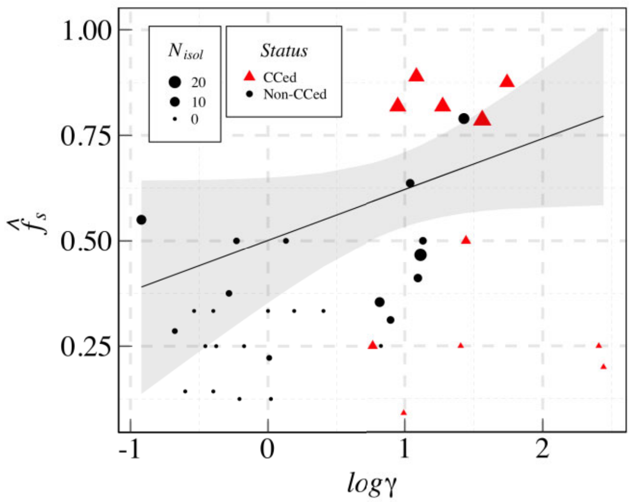

Figure 4. Relation between the fraction of isolated pulsar estimated by Laplace smoothing $\hat{f}_s$ and the disruption rate $\log \gamma$. The symbol sizes scale with the actual number of observed isolated pulsars. The straight line represents the best-fitting linear model with 95 per cent confidence band illustrated by the shaded region.

of linear regression is sensitive to the adopted smoothing parameter, we repeated the analysis by varying α from 2 to 5. We found that the results obtained from different α values all lie within the 95 per cent confidence band shown in Fig. 4 for the case of $\alpha = 1$.

3.2 Alternative classification by unsupervised clustering

While the aforementioned analyses show that P_{rot} and $L_{1.4\,GHz}$ of the MSPs in CCed GCs and non-CCed GCs are significantly different, the possible ambiguity in the conventional CCed/non-CCed classification can hamper the robustness of this conclusion. As we have mentioned in Section 2, such classification is determined by the structure of their brightness profiles. In case the central part of GC is poorly resolved, the CCed/non-CCed classifications are subjected to uncertainties.

This concern is reflected by the central concentration parameters c given in Harris (1996, 2010 edition), which is defined as the logarithm of the ratio between tidal radius r_t and core radius r_c. c is deduced from surface brightness profile fitting (King 1966; Trager et al. 1995). For most of the CCed GCs, no reasonable fit can be obtained and an upper bound of $c = 2.5$ is placed instead (cf. Trager et al. 1995; Harris 1996). While c can provide a simple parameter for characterizing the structure, we realize that our sample spans the ranges of $c = 0.79$–2.07 and $c = 1.63$–2.5 for non-CCed and CCed GCs, respectively. Such heavily overlapped ranges of c indicate the CCed/non-CCed classification in Harris (1996, 2010 edition) is not without ambiguity.

On the other hand, the disruption rates γ in Table 2 might provide a more quantitative measure of the dynamical status of a GC. For example, in Fig. 4, we have seen that the fraction of isolated pulsars f_s is generally correlated with γ, though the spread of the data from the best-fitting linear model is rather wide.

Individually, the parameters γ and c might not allow an unambiguous classification of GCs. This motivates us to examine whether the classification can be improved by combining both parameters.

For deriving the classification rules in the plane spanned by γ and c, we employed the Gaussian mixture model (GMM) algorithm. GMM is a probabilistic model with an assumption that the data

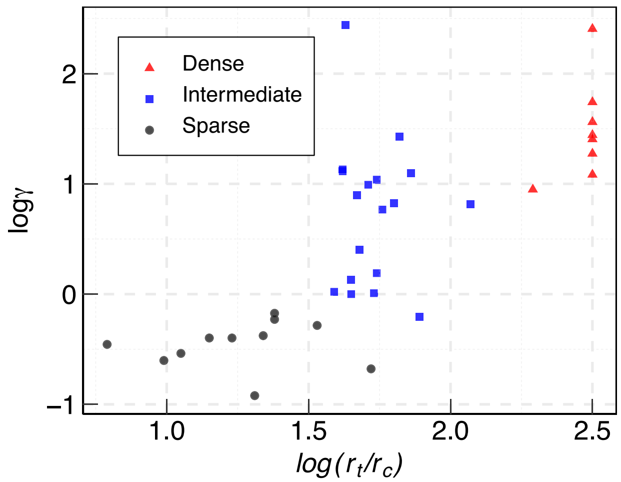

Figure 5. Unsupervised classification of GCs in a plane spanned by the disruption rate γ and the central concentration parameter c with the method of two-dimensional GMM.

originated from a mixture of finite numbers of Gaussian components. We have considered a set of models with the number of mixture components ranging from 1 to 9. We utilized the CRAN MCLUST package (version 5.4.6 Scrucca et al. 2016) for the model fitting and computed the likelihoods, L, of each model. Model selection is based on the Bayesian information criterion (BIC; Schwarz 1978): BIC $= 2\ln L - k\ln N$, where k and N are the number of estimated parameters and the sample size, respectively. We found that the optimal BIC requires three two-dimensional Gaussian components to model our adopted data in γ–c plane. In Fig. 5, three different groups as clustered by GMM are represented by the symbols of different colour. According to their brightness concentration, we refer to these groups as 'sparse (S)', 'intermediate (I)', and 'dense (D)' hereafter. The corresponding labels of each GC are given in Table 2. Under this classification scheme, S group consists of purely non-CCed GCs and D group only comprises CCed GCs. For the I group, there is a mixture of both non-CCed and CCed GCs.

These three groups in γ–c plane are well separated without much overlap (Fig. 5). The averaged isolated pulsars fractions $\langle f_s\rangle$ in S, I, and D groups are 0.64, 0.24, and 0.14, respectively, which increase progressively. These suggest such alternative classification is not unreasonable. This prompts us to re-examine the possible differences of pulsar properties among these three groups. The comparisons of their eCDFs of $P_{\rm rot}$, $P_{\rm b}$, $L_{1.4\,\rm GHz}$, and $L_{\rm X}$ are shown in Fig. 6. The corresponding p-values as inferred from the A–D test are summarized in Table 3.

In comparing $P_{\rm rot}$ between S group and D group, we found that the pulsars in D groups generally rotate slower than those in S group. Such a difference is statistically significant ($p = 7 \times 10^{-3}$). Also, the distribution of $L_{1.4\,\rm GHz}$ of S group is found to be significantly different from that of D group ($p = 0.013$) with the pulsars of D group significantly more luminous in L band than those of S group. These results are fully consistent with those inferred from the comparison between non-CCed and CCed populations as presented in Section 3.1 (cf. Fig. 1 and Table 1).

For I group, which consists of both non-CCed and CCed GCs, it is obvious that the $P_{\rm rot}$ distribution of I group is very similar to S group (see Fig. 6). Examining the composition of this group, we found that ∼90 per cent of the pulsars in I group are originated from non-CCed GCs that are dominated by the populations in 47 Tuc and Terzan 5. This might apparently account for the similarity. Nevertheless, despite the fact that the sample for $L_{1.4\,\rm GHz}$ in I group is also dominated by non-CCed pulsars that have a contribution of 83 per cent, its distribution is comparable to that of D group.

We would like to point out that the selection effect on the sample of $L_{1.4\,\rm GHz}$ might prevent us from drawing any firm conclusion in comparing this property among these three groups. While the sample size for $P_{\rm rot}$ is 279, there are only 59 pulsars that have their measures of $L_{1.4\,\rm GHz}$ available for analysis. This effect is particularly obvious in I group that has its sample size reduced from 179 for $P_{\rm rot}$ to 29 for $L_{1.4\,\rm GHz}$.This can be accounted for by the fact that only those sufficiently bright pulsars can have their radio fluxes reliably measured. It is uncertain whether the $L_{1.4\,\rm GHz}$ distribution of I group will remain comparable to D group when the fainter pulsars are included. Pulsar surveys with improved sensitivity might help to resolve this issue in the future.

4 SUMMARY AND DISCUSSION

Motivated by the recent work by Lee et al. (2023) that has identified the differences in various properties between the GC and GF pulsar populations, we proceed to investigate whether the variation of intracluster dynamics between CCed and non-CCed GCs can further diversify the pulsar properties (see Figs 1 and 2).

We found that pulsars in CCed GCs generally rotate slower than those in non-CCed GCs. This is consistent with the notion that secondary encounters in CCed GCs are enhanced (Verbunt & Freire 2014), which presumably results in the prevalence of isolated MSPs and fewer X-ray binaries than in non-CCed GCs with comparable primary encounter rates (Bahramian et al. 2013; Verbunt & Freire 2014; Kremer et al. 2022). The increased binary disruption efficiency in CCed GCs likely interrupts the angular momentum transfer at an earlier stage of recycling. Consequently, the slower rotation of pulsars in CCed GCs is not unexpected (see also Ivanova et al. 2008).

If the recycling process is halted at an earlier epoch, not only a slower rotating pulsar results, but we should also expect a stronger surface magnetic field than their counterparts in non-CCed GCs because the magnetic decay due to the mass transfer is suppressed (see the discussion in Lee et al. 2023). For pulsars, the strength of the dipolar surface magnetic field can be estimated by their rotational period $P_{\rm rot}$ and the corresponding spin-down rate $\dot{P}_{\rm rot}$, namely $B_{\rm s} \simeq \sqrt{\frac{3c^2 I}{2\pi^2 R_{\rm NS}^6}\dot{P}_{\rm rot}P_{\rm rot}}$, where c is the speed of light and $R_{\rm NS}$ is the radius of the neutron star. However, such estimation for the pulsars in GCs is complicated by the accelerations in the gravitational potential of a GC, which can bias the measurement of $\dot{P}_{\rm rot}$. Up to now, there are only a handful of GC pulsars with their intrinsic $\dot{P}_{\rm rot}$ estimated (cf. table 4 in Lee et al. 2023) and therefore we are not able to directly compare the $B_{\rm s}$ of the pulsars in CCed and non-CCed GCs.

On the other hand, as a pulsar radiates by tapping its rotational energy, the radiation power should be proportional to the spin-down power $\dot{E}$, which is expressed as $\dot{E} = 4\pi^2 I \dot{P}_{\rm rot} P_{\rm rot}^{-3} \propto B_{\rm s}^2 P_{\rm rot}^{-4}$, where I is the moment of inertia. Therefore, the radio luminosity $L_{1.4\,\rm GHz}$ can be treated as a proxy for probing $B_{\rm s}$ of the GC pulsars.

Our analysis indicates that $L_{1.4\,\rm GHz}$ of the pulsars in CCed GCs are significantly higher than those in non-CCed GCs (cf. Fig. 1). Together with the fact that $P_{\rm rot}$ of CCed GC pulsars are longer than those in non-CCed GCs, we can infer that $B_{\rm s}$ of CCed GC pulsars

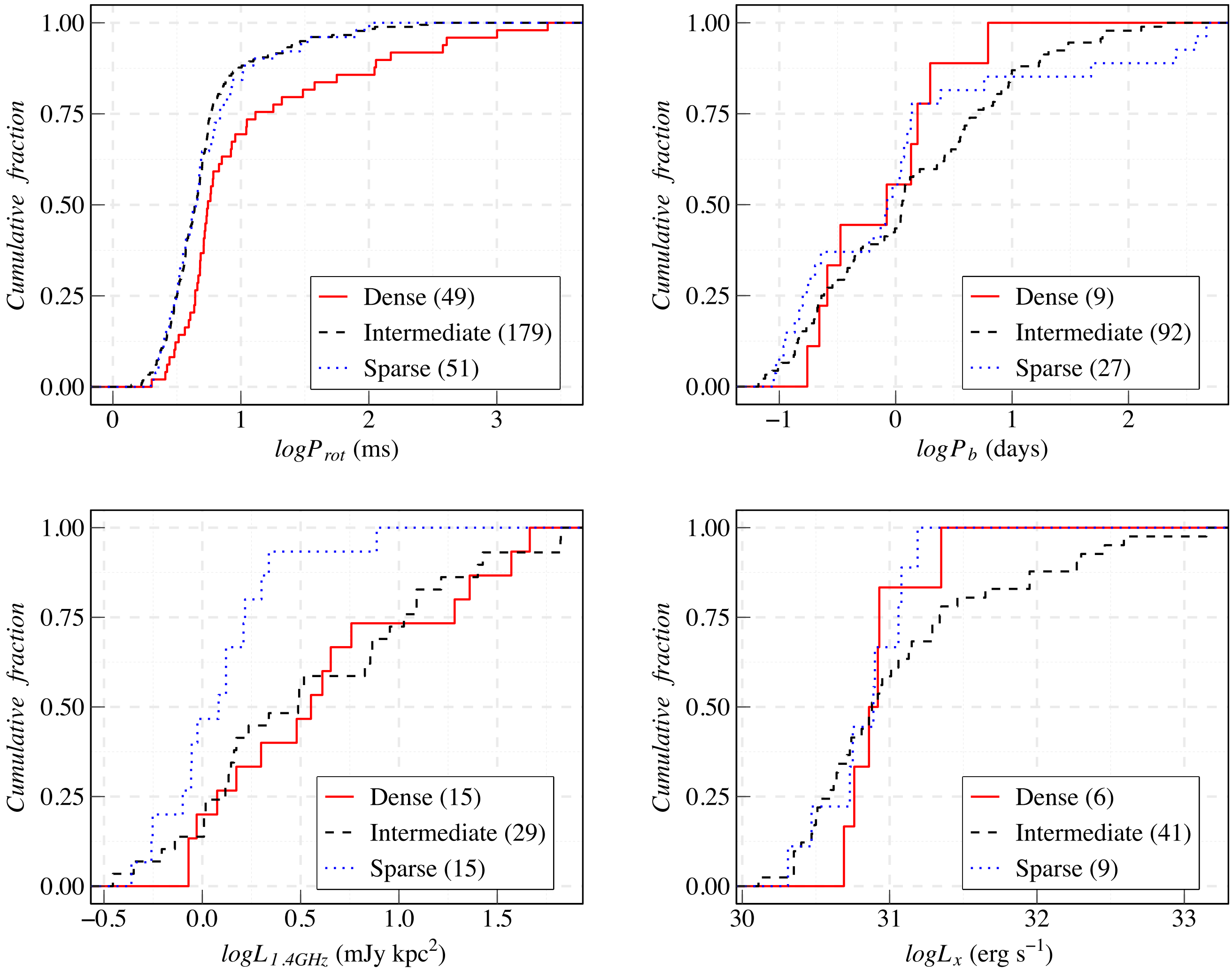

Figure 6. Comparisons of eCDFs of the selected pulsar properties among S, I, and D groups as determined by GMM. The numbers in parentheses in the legends show the corresponding sample sizes.

Table 3. Null hypothesis probabilities of the A–D test for comparing $P_{\rm rot}$, $P_{\rm b}$, $L_{1.4\,\rm GHz}$, and $L_{\rm X}$ among S, I, and D groups as classified by GMM.

	S versus D	S versus I	D versus I
$P_{\rm rot}$	0.007	0.898	0.0002
$P_{\rm b}$	0.612	0.214	0.472
$L_{1.4\,\rm GHz}$	0.013	0.012	0.902
$L_{\rm X}$	0.844	0.522	0.406

are stronger than those in non-CCed GCs, which is in line with our aforementioned speculation.

To investigate whether the difference in $L_{1.4\,\rm GHz}$ is genuine, we have further checked whether such a difference can be a result of the observational effect. If a GC is close to us, a flux-limited survey will uncover more faint sources than those in the more distant GCs. For examining this issue, we compared the distances d between the CCed and non-CCed GCs in our sample, and the results are shown in Fig. 7. The medians of d of CCed and non-CCed GCs are 6.8 and 6.9 kpc, respectively. With the A–D test, we do not find any significant difference between these two eCDFs ($p > 0.05$). Hence,

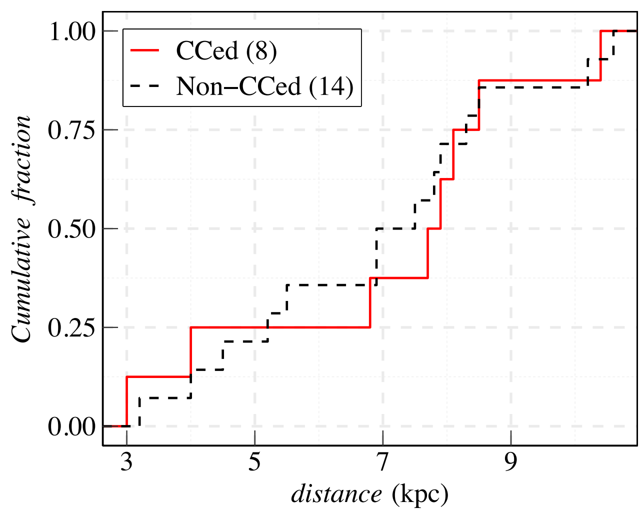

Figure 7. Comparison of eCDFs of the distance between CCed GCs and non-CCed GCs in our sample.

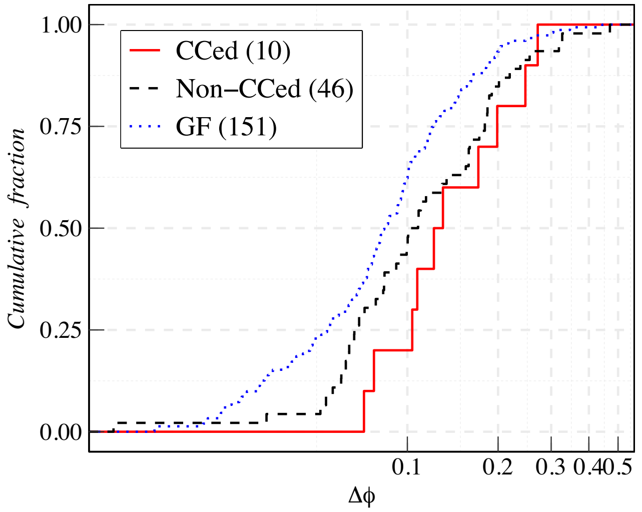

Figure 8. Comparison of eCDFs of the estimates of radio beam sizes $\Delta\phi$ of MSPs in CCed GCs, non-CCed GCs, and the GF.

we conclude that the difference in $L_{1.4\,\mathrm{GHz}}$ between CCed and non-CCed GCs is genuine.

On the other hand, the A–D test indicates that the differences in $L_{1.4\,\mathrm{GHz}}$ and L_{X} between the GF and GC MSP populations are statistically significant. However, we notice that many GF MSPs are located in our proximity. The medians of d for radio-selected MSPs in GCs and GF in our sample are found to be 6.9 and 1.7 kpc, respectively. The A–D test yields a p-value of $\sim 10^{-22}$, which indicates a very significant difference between their distributions of d. Consequently, the excess at the lower end of the distribution of $L_{1.4\,\mathrm{GHz}}$ for GF MSPs (Fig. 2) can be a result of observational bias. This bias also affects the comparison of L_{X} between MSPs in GCs (median $d = 4.9$ kpc) and GF (median $d = 1.2$ kpc) in our sample.

In conclusion, our results demonstrate that CCed and non-CCed GC pulsar populations exhibit differences in their rotation rates and radio luminosities, with CCed GC pulsars rotating slower and having higher radio luminosities. This supports the idea that the recycling process is halted earlier in CCed GCs, leading to stronger surface magnetic fields and slower rotations.

For further examining the effect of dynamical effects on the structure of the surface magnetic field, we would like to compare the radio beam sizes of MSPs in GF, CCed GCs, and non-CCed GCs. The beam sizes can be estimated by $\Delta\phi = W_{50}/P_{\mathrm{rot}}$, where W_{50} is the pulse width at 50 per cent of the peak in the unit of time as obtained from the ATNF catalogue (Manchester et al. 2005). The comparisons of $\Delta\phi$ among three populations are given in Fig. 8.

It is interesting to note that the $\Delta\phi$ of MSPs in GF is smaller than those in non-CCed and CCed GCs. With the A–D test, we find $\Delta\phi$ of the GF population is significantly smaller than those of non-CCed MSPs (p-value $\sim$0.01) and CCed MSPs (p-value $\sim$0.02). We also note that the $\Delta\phi$ from non-CCed GCs is apparently smaller than that from CCed GCs, although the A–D test does not yield a p-value below our pre-defined criterion.

These results conform with the expectation that different recycling histories can lead to different surface magnetic field structures. Chen & Ruderman (1993) argued that mass accretion could reduce the polar cap radius and hence the size of the open field line region. This notion is supported by Kramer et al. (1998), who found that the open angle of GF MSPs is smaller than that expected from the dipolar geometry (cf. fig. 12 in their paper).

The fact that the $\Delta\phi$ of GF MSPs is smaller than those of GC MSPs is consistent with the scenario that the accretion phase of GC MSPs is shortened by dynamical disruption, as suggested by Lee et al. (2023). Since the disruption rate is generally higher in CCed GCs (see Table 2 and Fig. 4), the MSPs in CCed GCs should have a larger beam size than those in non-CCed GCs. However, a firm conclusion is precluded by the current sample size. With more samples available in the future, the comparison of $\Delta\phi$ between these two classes of GC MSPs should be revisited.

We have to point out a caveat in the comparison of $\Delta\phi$ presented here. First, owing to the complexity of the radio pulse profile, W_{50} should be considered as a poor estimator for the size of the emission beam. Second, beam size should be a function of observing frequency. However, such information is not available in the ATNF catalogue. A more accurate determination of the emission geometry should be derived from fitting the polarization data. Therefore, we strongly encourage a dedicated study to compare the emission geometry of MSPs in GF and GCs with radio polarization, which can help to scrutinize our hypothesis.

Finally, we would like to emphasize that all the aforementioned discussions are based on the conventional CCed/non-CCed classification of GCs, which relies on photometric measurements (Trager et al. 1995; Harris 1996). In Section 3.2, we have pointed out a possible ambiguity of this conventional classification scheme. Bianchini et al. (2018) have also mentioned that there is no robust connection between the photometric central concentration and the dynamical state of a GC.

By combining the central concentration parameter c and a dynamical measure of disruption rate γ, we have shown that the GCs in our sample can be divided into three groups (Fig. 5). For two groups maximally separated in the γ–c plane, namely S group and D group, they purely comprised non-CCed GCs and CCed GCs, respectively (cf. Table 2). By comparing the distributions of P_{rot} and $L_{1.4\,\mathrm{GHz}}$ between these two groups, the differences remain to be statistically significant. On the other hand, the I group has a mixture of CCed and non-CCed GCs. Both flux-limited samples and a strong bias in the I group by the pulsars from a few non-CCed GCs (e.g. 47 Tuc and Terzan 5) preclude any conclusive comparison with the other two groups.

This has also raised a concern that the classification scheme of GCs might not be unique. In view of the complex evolution of GCs (e.g. Ivanova et al. 2006; Hong et al. 2017), the description of both dynamical status and structure of GCs can be more complicated than the binary classification as simple as CCed or non-CCed. For example, by examining the radial distribution of blue stragglers, Ferraro et al. (2012) have shown that the dynamical age of GCs can be divided into three groups. With a more comprehensive classification scheme proposed by further studies, the differences in pulsar properties among different groupings can be re-examined.

ACKNOWLEDGEMENTS

KO was supported by the National Research Foundation of Korea grants 2022R1F1A1073952 and 2022R1A6A3A13071461. CYH was supported by the research fund of Chungnam National University and by the National Research Foundation of Korea grant 2022R1F1A1073952. JT was supported by the National Key Research and Development Program of China (grant no. 2020YFC2201400) and the National Natural Science Foundation of China (NSFC, grant no. 12173014). AKHK was supported by the National Science and Technology Council of Taiwan through grant 111-2112-M-007-020. PHT was supported by NSFC grant no. 12273122 and the China Manned Space Project (no. CMS-

CSST-2021-B09). KLL was supported by the National Science and Technology Council of the Republic of China (Taiwan) through grant 111-2636-M-006-024, and he is also a Yushan Young Fellow supported by the Ministry of Education of the Republic of China (Taiwan).

DATA AVAILABILITY

The data underlying this article were accessed from Chandra Data Archive (https://cda.harvard.edu/chaser/) and ATNF (https://www.atnf.csiro.au/research/pulsar/psrcat/).

REFERENCES

Alpar M. A., Cheng A. F., Ruderman M. A., Shaham J., 1982, Nature, 300, 728
Bahramian A., Heinke C. O., Sivakoff G. R., Gladstone J. C., 2013, ApJ, 766, 136
Bianchini P., Webb J. J., Sills A., Vesperini E., 2018, MNRAS, 475, L96
Chen K., Ruderman M., 1993, ApJ, 408, 179
Clark G. W., 1975, ApJ, 199, L143
Cumming A., Arras P., Zweibel E., 2004, ApJ, 609, 999
Fabian A. C., Pringle J. E., Rees M. J., 1975, MNRAS, 172, 15
Fabian A. C., Pringle J. E., Verbunt F., Wade R. A., 1983, Nature, 301, 222
Ferraro F. R. et al., 2012, Nature, 492, 393
Fregeau J. M., Rasio F. A., 2007, ApJ, 658, 1047
Gelman A., Carlin J., Stern H., Dunson D., Vehtari A., Rubin D., 2013, Bayesian Data Analysis, 3rd edn. Taylor and Francis, CRC Press, United States
Harris W. E., 1996, AJ, 112, 1487
Hong J., Vesperini E., Belloni D., Giersz M., 2017, MNRAS, 464, 2511
Hui C. Y., Li K. L., 2019, Galaxies, 7, 93
Hui C. Y., Cheng K. S., Taam R. E., 2010, ApJ, 714, 1149
Ivanova N., Heinke C. O., Rasio F. A., Taam R. E., Belczynski K., Fregeau J., 2006, MNRAS, 372, 1043
Ivanova N., Heinke C. O., Rasio F. A., Belczynski K., Fregeau J. M., 2008, MNRAS, 386, 553
Katz J. I., 1975, Nature, 253, 698
King I. R., 1966, AJ, 71, 64
Kramer M., Xilouris K. M., Lorimer D. R., Doroshenko O., Jessner A., Wielebinski R., Wolszczan A., Camilo F., 1998, ApJ, 501, 270
Kremer K., Ye C. S., Kıroğlu F., Lombardi J. C., Ransom S. M., Rasio F. A., 2022, ApJ, 934, L1
Lee H. M., Ostriker J. P., 1986, ApJ, 310, 176
Lee J., Hui C. Y., Takata J., Kong A. K. H., Tam P.-H. T., Li K.-L., Cheng K. S., 2023, ApJ, 944, 225
Lombardi J. C., Jr, Proulx Z. F., Dooley K. L., Theriault E. M., Ivanova N., Rasio F. A., 2006, ApJ, 640, 441
Lynden-Bell D., Wood R., 1968, MNRAS, 138, 495
Manchester R. N., Hobbs G. B., Teoh A., Hobbs M., 2005, AJ, 129, 1993
Manning C. D., Raghavan P., Schütze H., 2008, Introduction to Information Retrieval. Cambridge Univ. Press, Cambridge
Pooley D. et al., 2003, ApJ, 591, L131
Press W. H., Teukolsky S. A., 1977, ApJ, 213, 183
Radhakrishnan V., Srinivasan G., 1982, Curr. Sci., 51, 1096
Rivera Sandoval L. E. et al., 2018, MNRAS, 475, 4841
Schwarz G., 1978, Ann. Stat., 6, 461
Scrucca L., Fop M., Murphy T. B., Raftery A. E., 2016, R J., 8, 289
Sigurdsson S., Phinney E. S., 1995, ApJS, 99, 609
Trager S. C., King I. R., Djorgovski S., 1995, AJ, 109, 218
Verbunt F., Freire P. C. C., 2014, A&A, 561, A11
Ye C. S., Kremer K., Chatterjee S., Rodriguez C. L., Rasio F. A., 2019, ApJ, 877, 122
Ye C. S., Kremer K., Rodriguez C. L., Rui N. Z., Weatherford N. C., Chatterjee S., Fragione G., Rasio F. A., 2022, ApJ, 931, 84

This paper has been typeset from a TEX/LATEX file prepared by the author.